

Glassy dynamics of model colloidal polymers: Effect of controlled chain stiffness

Jian Li(李健), Bo-kai Zhang(张博凯), and Yu-Shan Li(李玉山)

Citation: Chin. Phys. B, 2021, 30 (**3**): 036104. DOI: 10.1088/1674-1056/abd6f8
Journal homepage: http://cpb.iphy.ac.cn; http://iopscience.iop.org/cpb

What follows is a list of articles you may be interested in

Understanding defect production in an hcp Zr crystal upon irradiation: An energy landscape perspective

Jiting Tian(田继挺)
Chin. Phys. B, 2021, 30 (**2**): 026102. DOI: 10.1088/1674-1056/abbbe0

Nearly golden-ratio order in Ta metallic glass

Yuan-Qi Jiang(蒋元祺), Ping Peng(彭平)
Chin. Phys. B, 2020, 29 (**4**): 046105. DOI: 10.1088/1674-1056/ab773f

Fractional variant of Stokes-Einstein relation in aqueous ionic solutions under external static electric fields

Gan Ren(任淦), Shikai Tian(田时开)
Chin. Phys. B, 2020, 29 (**3**): 036101. DOI: 10.1088/1674-1056/ab695b

Supercooled liquids analogous fractional Stokes-Einstein relation in NaCl solution above room temperature

Gan Ren(任淦), Shikai Tian(田时开)
Chin. Phys. B, 2019, 28 (**7**): 076107. DOI: 10.1088/1674-1056/28/7/076107

Structural evolution in deformation-induced rejuvenation in metallic glasses: A cavity perspective

Shaoqin Jiang(江少钦), Yong Huang(黄勇), Maozhi Li(李茂枝)
Chin. Phys. B, 2019, 28 (**4**): 046103. DOI: 10.1088/1674-1056/28/4/046103

Glassy dynamics of model colloidal polymers: Effect of controlled chain stiffness*

Jian Li(李健)[1], Bo-kai Zhang(张博凯)[2,†], and Yu-Shan Li(李玉山)[1,‡]

[1] *Department of Physics and Electronic Engineering, Heze University, Heze* 274015, *China*
[2] *Department of Physics, Zhejiang Sci-Tech University, Hangzhou* 310018, *China*

(Received 11 November 2020; revised manuscript received 20 December 2020; accepted manuscript online 28 December 2020)

Colloidal polymers with tunable chain stiffness have been successfully assembled in experiments recently. Similar to molecular polymers, chain stiffness is an important feature which can distinctly affect the dynamical behaviors of colloidal polymers. Hence, we model colloidal polymers with controlled chain stiffness and study the effect of chain stiffness on glassy behaviors. For stiff chains, there are long-ranged periodic intrachain correlations besides two incompatible local length scales, i.e., monomer size and bond length. The mean square displacement of monomers exhibits sub-diffusion at intermediate time/length scale and the sub-diffusive exponent increases with chain stiffness. The data of localization length of stiff polymers versus rescaled volume fraction for different monomer sizes can gather close to an exponential curve and decay slower than those of flexible polymers. The increase of chain stiffness linearly increases the activation energy of the colloidal-polymer system and thus makes the colloidal polymers vitrify at lower volume fraction. Static and dynamic equivalences between stiff colloidal polymers of different monomer sizes have been checked.

Keywords: glassy dynamics, colloidal polymers, molecular dynamics, mean square displacement

PACS: 61.43.Fs, 64.70.Kj, 64.70.Km, 64.70.Pj **DOI:** 10.1088/1674-1056/abd6f8

1. Introduction

Polymers are among the most studied materials for slow dynamics and glass transitions since they are difficult to crystallize due to their chain structure.[1–5] Lots of theoretical and numerical works have been devoted to fundamentally understanding their nonequilibrium slow dynamics and topological properties.[6–11] Chain structure and intramolecular barrier are two important polymer-specific features which cause the distinct dynamical behaviors of polymer melt from those of molecular liquids. For example, chain connectivity causes Rouse-like sub-diffusive motion of monomers at intermediate time.[7,12–14] Additionally, the intramolecular barrier plays an important role in glass transitions of polymers. Simulations and mode coupling theory (MCT) calculations on bead-spring chains found that the increase of the intramolecular barrier strength increases the MCT exponent and MCT critical temperature.[15–20]

In recent years, attempts have been made to assemble "colloidal monomers," e.g., inorganic nanoparticles, into chain structures, termed "colloidal polymers" or "nanopolymers" or "nanochains."[21] Colloidal polymers combine the features of both colloids (e.g., the large size of elements) and molecular polymers (e.g., the chain connectivity). Importantly, colloidal polymers provide a tool to observe glass transition in the real space with confocal microscope. In experiments, colloidal monomers form colloidal chains through attractive, directional, interparticle interactions, which are similar to covalent or supramolecular interactions in molecular chains.[21] In contrast to the high degree of structural control available in the synthesis of molecular polymers, methods to control fundamental structural features of colloidal polymers are still being developed.[22–26] However, colloidal polymers with tunable chain stiffness have been successfully assembled in experiments.[27–29] Similar to molecular polymers, chain stiffness can play an important role in glass transitions and slow dynamics of colloidal polymers. This stimulates us to study the effect of chain stiffness on glassy dynamics of colloidal polymers.

In our previous work,[30] we proposed a model to address the large monomer size of flexible colloidal polymers and study their glassy dynamics. We focused on the quantitative differences in the static structure and slow dynamics as the polymers vary from molecular chains to colloidal chains. Here, we build a model of colloidal polymer with controlled chain stiffness. By the new model, we employ molecular dynamic (MD) simulations to investigate the slow dynamics of the dense systems composed of colloidal polymers with controlled chain stiffness. The Newtonian dynamics is adopted instead of Brownian dynamics, because (1) the microscopic law of motion does not essentially influence the long-time glassy behavior;[31–34] (2) we can thus use velocity-Verlet algorithm and large time step, i.e., it is computationally more efficient.

*Project supported by the National Natural Science Foundation of China (Grant Nos. 11804085 and 11847115) and the Doctoral Foundation of Heze University (Grant No. XY18BS13).

†Corresponding author. E-mail: bkzhang@zstu.edu.cn
‡Corresponding author. E-mail: lysh507@163.com

© 2021 Chinese Physical Society and IOP Publishing Ltd

The paper is organized as follows. We describe our colloidal polymer model with controlled chain stiffness and simulation method in Section 2. The results and discussion are given in Section 3. In Subsection 3.1, we report the results of static structure, including intrachain pair correlation and radial distribution function. The dynamic properties are reported in Subsections 3.2 and 3.3, such as the mean squared displacement, localization length, and Characteristic time. Finally, static and dynamic equivalences are discussed in Subsection 3.4. We summarize the paper in Section 4.

2. Model and simulation details

We use the purely repulsive Weeks–Chandler–Anderson potential, which is shifted to the surface (WCAS), to model the monomer–monomer excluded-volume interaction[35]

$$U_{\mathrm{WCAS}}(r) = \begin{cases} \infty, & r \le \Delta, \\ 4\varepsilon\left[\left(\dfrac{\sigma}{r-\Delta}\right)^{12} - \left(\dfrac{\sigma}{r-\Delta}\right)^{6}\right] + \varepsilon, & \Delta < r \le r_{\mathrm{c}} + \Delta, \\ 0, & r > r_{\mathrm{c}} + \Delta, \end{cases} \tag{1}$$

where r is the center-to-center distance between monomers, σ is the Lennard–Jones (LJ) diameter, and ε is the characteristic energy. The potential is cut off at $r_{\mathrm{c}} = 2^{1/6}\sigma$. Δ is the diameter of the hard core of the colloidal monomers. Similar potential has already been used to study the self-assembling of polymer-tethered nanospheres and nanorods.[35] We change Δ to modify the monomer size. The potential reduces to the common WCA potential for molecular monomers when $\Delta = 0$. We define the nominal diameter of monomers as $\sigma_{\mathrm{p}} = \Delta + r_{\mathrm{c}}$, which is adjustable by the value of Δ. We adopt the LJ units, i.e., $\varepsilon = 1$, $\sigma = 1$, the Boltzmann's constant $k_{\mathrm{B}} = 1$, and the monomer mass $m = 1$.

In addition to U_{WCAS}, the bond connection between successive monomers along the chain is modeled by the finitely extensible nonlinear elastic springs (FENESs),[36] which is also shifted to the surface,

$$U_{\mathrm{FENES}}(r) = -0.5KR_0^2 \ln\left[1 - \left(\frac{r-\Delta}{R_0}\right)^2\right]. \tag{2}$$

The parameters $K = 30$ and $R_0 = 1.5$. The composition of the WCAS potential and the FENES potential yields the effective bond potential with a sharp minimum at $r_{\mathrm{b}} = \Delta + 0.9606$. The bonded and non-bonded potentials prevent the chains from crossing. The incompatible length scales (σ_{p} and r_{b}) and the flexibility of the chains make the system avoid crystallization.[6] Therefore, contrary to the colloidal system, polydispersity of monomer sizes is not required to generate the amorphous state at high volume fractions.

From the view of coarse-grained model, the major feature of colloidal polymers that is different from molecular polymers is the large monomer size (large repulsive core). In experiments, the colloidal polymers can be assembled through nanoparticles linked by coated polymer shell and the monomer size of the colloidal polymers typically varies from 5 nm to 60 nm.[21,23] Our model corresponds to this case of nanoparticles linked by coated polymer shell. $\Delta + r_{\mathrm{c}}$ is varied to represent the different sizes of the repulsive core.

The chain stiffness is controlled by a cosine harmonic bending potential, which acts on three consecutive monomers along the chain,

$$V_{\mathrm{B}}(\theta_i) = \frac{1}{2}k_\theta(\cos\theta - \cos\theta_0)^2, \tag{3}$$

where θ is the bending angle between consecutive monomers $i-1$, i, and $i+1$ ($2 \le i \le N-1$). The angle between adjacent pairs of bonds is maintained close to the equilibrium value $\theta_0 = 180^\circ$, which can effectively represent the monomer directionality of the colloidal polymers. Additionally, the bending constant k_θ is varied to obtain different chain stiffnesses. The intuitive diagram of the chain of three monomers is shown in Fig. 1, and the parameters σ_{p}, r_{b}, and θ are marked.

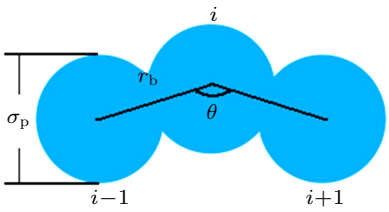


Fig. 1. The intuitive diagram of the chain of three monomers.

We perform MD simulations of a system containing $n = 200$ chains of $N = 10$ monomers. The cubic simulation volume V is used as an adjustable parameter to obtain different volume fractions, which is defined as $\phi = 1000\pi\sigma_{\mathrm{p}}^3/3V$, where $\sigma_{\mathrm{p}} = \Delta + r_{\mathrm{c}}$ is the nominal diameter of the monomers. The monomer is the coarse-grained soft particle. Furthermore, the bond length r_{b} is a little smaller than nominal diameter σ_{p}. Hence, the maximal volume fraction reaches to 0.89 in our simulations, which is larger than the hard-sphere close-packed volume fraction 0.74. The reduced temperature is fixed at $T^* = 1.0$. In the simulation, the canonical ensemble (NVT) with the Nose–Hoover thermostat is adopted for runs to equilibrium, then the microcanonical ensemble (NVE) is used in the production runs. The equations of motion for the NVE are integrated by the velocity-Verlet algorithm with time step of $0.001\tau_{\mathrm{LJ}}$, where the time scale $\tau_{\mathrm{LJ}} = \left(m\sigma^2/\varepsilon\right)^{1/2}$. At least ten independent configurations are simulated for each set of system parameters. Three monomer sizes are considered: $\sigma_{\mathrm{p}} = 2^{1/6}$, 2, and 4, and the bending constants $k_\theta = 0$, 5, 15, 25, 30 are used to obtain five chain stiffnesses for each momomer size ($k_\theta = 0$ corresponding to the flexible chain).

3. Results and discussion

3.1. The static structural properties

The static structural properties of five chain stiffnesses for $\sigma_p = 4.0$ and $\phi = 0.575$ are shown in Fig. 2. The main peak of the radial distribution function (RDF) $g(r)$ splits into two as a consequence of two incompatible local length scales, i.e., monomer size and bond length (Fig. 2(a)). The strongest peak is located near r_b/σ_p, contributed mostly by the jointed monomers, while the shoulder peak appears at r/σ_p closer to 1, reflecting the characteristic distance of the excluded volume interaction between monomers. For stiff chains, i.e., $k_\theta \neq 0$, a sharp maximum appears in the second peak of $g(r)$. The reduced position and height of the sharp maximum shift differently to smaller and larger values for larger bending constant. The average intrachain pair correlation function $\omega(r)$ and histogram of bending angle $n(\theta)$ (inset) are shown in Fig. 2(b). The position of the first peak of $\omega(r)$ corresponds to the distance between the jointed monomers too. $\omega(r)$ decays rapidly with r for flexible chains, reflecting that the intrachain correlation is very short-ranged. However, $\omega(r)$ exhibits long-ranged periodic decayed peaks with r for stiff chains, and the position and height of the same-order peak shift to larger values for larger bending constant. The characteristic length between the $(i-1)$th and $(i+1)$th monomers in a chain can be reflected by the peak's position of the histogram of bending angle (Fig. 2(b) inset). For flexible chains, i.e., $k_\theta = 0$, two peaks emerge in the histograms of bending angles, which means there are two characteristic lengths. The positron of the first strong peak represents the characteristic length near σ_p, and the position of the second weak peak is close to that of the only peak of stiff chains. For stiff chains, the position of the only peak represents the characteristic length shifted to $2r_b$, and the position and height of the peak also shift to larger values for larger bending constant.

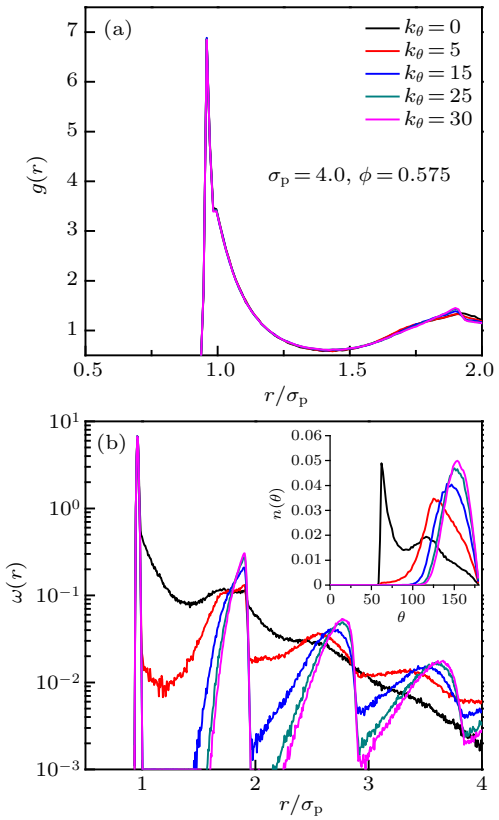


Fig. 2. The static structural properties of five chain stiffnesses for monomer-size and volume-fraction combination $\sigma_p = 4.0$, $\phi = 0.575$. (a) The radial distribution function $g(r)$. (b) The intrachain pair correlation function $\omega(r)$ and the inset shows the histogram of bending angle $n(\theta)$.

3.2. The mean square displacement

The mean square displacement (MSD) of monomers is defined as

$$\left\langle r^2(t)\right\rangle = \frac{1}{nN} = \sum_{i=1}^{n}\sum_{j=1}^{N}\left\langle \left(\boldsymbol{r}_{ij}(t) - \boldsymbol{r}_{ij}(0)\right)^2\right\rangle, \tag{4}$$

where $\boldsymbol{r}_{ij}$ is the position of the monomer j in the ith chain. The MSD of five chain stiffnesses for two monomer-size and volume-fraction combinations is shown in Fig. 3. For flexible chains, three regimes are observed: ballistic regime, Rouse-like subdiffusive regime, and normal diffusive regime. For stiff chains, a caging regime with significant smaller exponent or a horizontal plateau emerges after the ballistic motion, indicating the phenomenon of localization. At long time, MSD restores the sub-diffusive motion. The Rouse-like sub-diffusion of flexible chains happens in the displacement range between bond length r_b and end-to-end distance R_e. These two lengths (squared) are marked out in Fig. 3 as dashed lines. R_e varies largely with chain stiffness, e.g., for combination $\sigma_p = 2^{1/6}$, $\phi = 0.78$, $R_e = 3.5$ when $k_\theta = 0$ and $R_e = 6.7$ when $k_\theta = 30$; for combination $\sigma_p = 4.0$, $\phi = 0.575$, $R_e = 13.6$ when $k_\theta = 0$ and $R_e = 26.2$ when $k_\theta = 30$. The sub-diffusion of monomers and diffusion of chains in polymer melts depend on many factors such as chain architecture, chain stiffness, chain length, and intrachain excluded volume interaction.[37–41] Different sub-diffusive regimes of monomers have been observed.[37–39] For our model of colloidal polymers, we find that the sub-diffusive exponent α depends on the chain stiffness, which increases from 0.63 to 0.78 with the bending constant k_θ (see Fig. 3(c)).

The MSD of monomers of stiff chains with bending constant $k_\theta = 25$ for two monomer sizes at various momomer volume fractions is shown in Fig. 4. At low volume fractions, the ballistic regime, subdiffusive regime, and normal diffusive regime are observed. At high volume fractions, a caging regime with significant smaller exponent merges after the ballistic motion, then MSD restores the sub-diffusive motion at long time. The square bond length (r_b^2) and end-to-end distance of chains (R_e^2) are also marked by dashed lines. R_e varies slightly with the volume fraction. From Fig. 4(c), it is found

that the sub-diffusive exponent $\alpha \sim 0.75$ is independent of the volume fractions and monomer sizes.

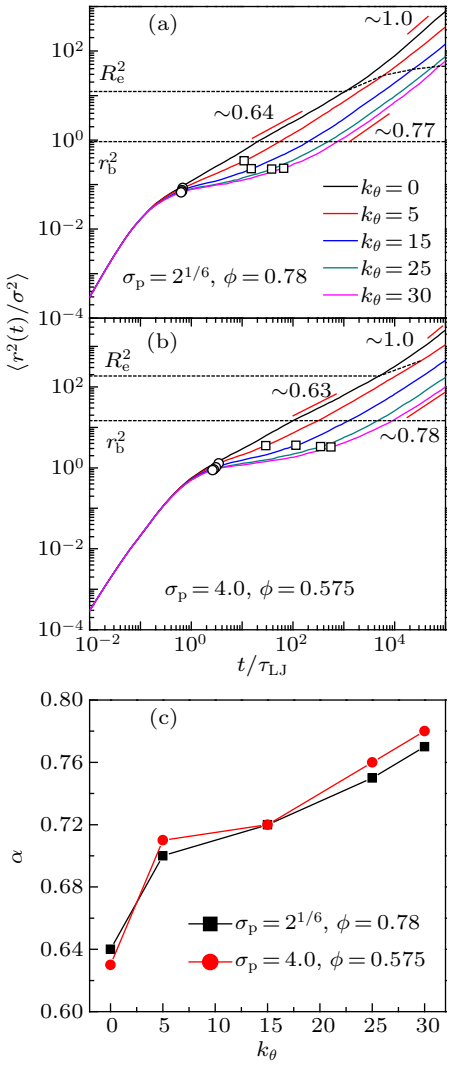


Fig. 3. Mean square displacement $\langle r^2(t)/\sigma^2 \rangle$ of monomers for five chain stiffnesses. (a) The monomer-size and volume-fraction combinations $\sigma_p = 2^{1/6}$, $\phi = 0.78$. (b) $\sigma_p = 4.0$, $\phi = 0.575$. The end points between ballistic and caging regimes are marked with open circles and those between caging and sub-diffusive regimes are marked with open squares. The square bond length (r_b^2) and end-to-end distance of chains (R_e^2) are marked out as dashed lines. (c) The sub-diffusive exponent α as a function of bending constant k_θ for two monomer-size and volume-fraction combinations.

To characterize the length scales of localization,we mark the two end-points of the caging regime,[42] as shown in Figs. 4(a) and 4(b), to represent the crossed points from ballistic motion to caging and from caging to sub-diffusion. At $\phi = \phi^*$, the two end-points merge, and ϕ^* is the threshold volume fraction beyond which caging dynamics emerges in stiff colloidal polymers. We obtain $\phi^* \approx 0.65$ for $\sigma_p = 2^{1/6}$, $\phi^* \approx 0.55$ for $\sigma_p = 2$, and $\phi^* \approx 0.49$ for $\sigma_p = 4$. At the threshold volume fraction ϕ^*, the height of the merged point gives an estimate of the localization length $\sqrt{6} r_{loc}^* = \sqrt{\langle r^2(t) \rangle^*}$.[43] We have $r_{loc}^*/\sigma_p \approx 0.23$, larger than the Lindemann melting criterion which is about 10%,[44] and also larger than the case of flexible chains which is about 0.14.[30] At $\phi > \phi^*$, we choose the middle point between the two end points in terms of $\log(t)$.[45] The height of this middle point gives an estimate of the characteristic localization length $\sqrt{6} r_{loc}$. The localization length decreases roughly exponentially with the increase of the volume fraction.[46] When the volume fraction is rescaled by ϕ^*, we find that the data of localization length versus volume fraction for different monomer sizes gather close to the curve $r_{loc}/\sigma_p \approx 15.61 \exp(-3.33\phi/\phi^*)$ (solid line in Fig. 5). The height of the end-point between caging and sub-diffusion gives an estimate of the typical typical length R, beyond which the monomer can escape the cage. The data of R for different monomer sizes gather close to the curve $R/\sigma_p \approx 10.96 \exp(-2.75\phi/\phi^*)$ (dashed line in Fig. 5). r_{loc} and R both decay slower than those of flexible chains.[30]

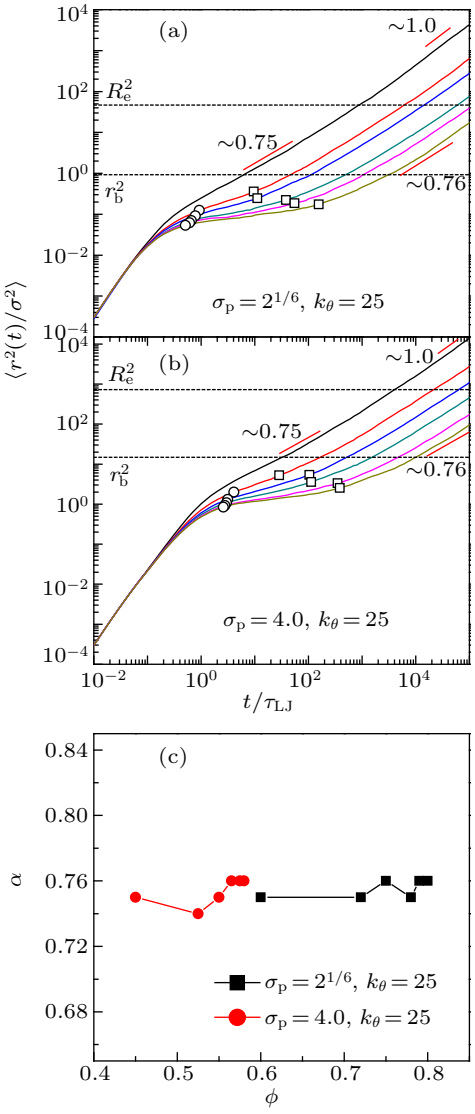


Fig. 4. Mean square displacement $\langle r^2(t)/\sigma^2 \rangle$ of monomers for stiff chains with bending constant $k_\theta = 25$. (a) The monomer size $\sigma_p = 2^{1/6}$ and the volume fractions are (from top to bottom) 0.60, 0.72, 0.75, 0.78, 0.79, 0.80. (b) The monomer size $\sigma_p = 4.0$ and the volume fractions are (from top to bottom) 0.45, 0.525, 0.55, 0.565, 0.575, 0.58. The end points between ballistic and caging regimes are marked with open circles and those between caging and sub-diffusive regimes are marked with open squares. The square bond length (r_b^2) and end-to-end distance of chains (R_e^2) are marked out as dashed lines. (c) The sub-diffusive exponent α as a function of volume fraction ϕ for two monomer-size and bending-constant combinations.

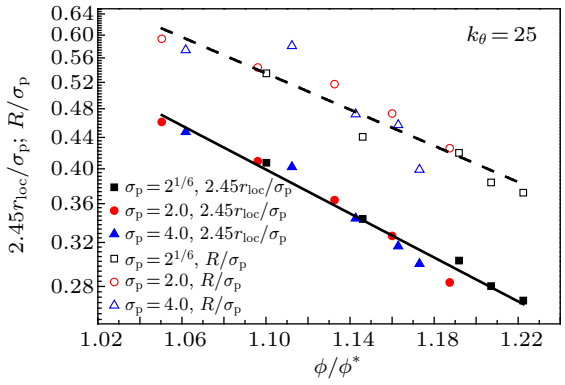


Fig. 5. Log-linear plot of $\sqrt{6}r_{loc}/\sigma_p$ (solid symbols) and R/σ_p (open symbols) as functions of scaled volume fraction ϕ/ϕ^* for stiff chains with bending constant $k_\theta = 25$. Two lines represent exponential relations $r_{loc}/\sigma_p \approx 15.61\exp(-3.33\phi/\phi^*)$ (solid line) and $R/\sigma_p \approx 10.96\exp(-2.75\phi/\phi^*)$ (dashed line).

3.3. Characteristic time

Slow dynamics of glass forming liquids is often analyzed by the intermediate (self-) scattering function

$$F_s(q,t) = \frac{1}{nN}\sum_{i=1}^{n}\sum_{j=1}^{N}\left\langle \exp\left[i\boldsymbol{q}\cdot(\boldsymbol{r}_{ij}(0)-\boldsymbol{r}_{ij}(t))\right]\right\rangle. \quad (5)$$

Such correlation function accounts for the loss in time of the memory of the initial structural configuration. Usually, the q is chosen to be the position of the first peak of the static structure factor. The $F_s(q,t)$ for two monomer-size and volume-fraction combinations at five bending constants is shown in Fig. 6(a). For the two combinations, the $F_s(q,t)$ decays slower as the increase of bending constants. We define the α relaxation time τ_α as when $F_s(q,t=t_\alpha) = 0.1$. At long time, i.e., $F_s(q,t) < 0.2$, the decay of $F_s(q,t)$ displays good time-(volume fraction) and time-(monomer size) superposition for stiff chains (see Fig. 6(b)), which is in agreement with that of flexibale chains.[30] At short time, a two-step decay (caging) is observed.

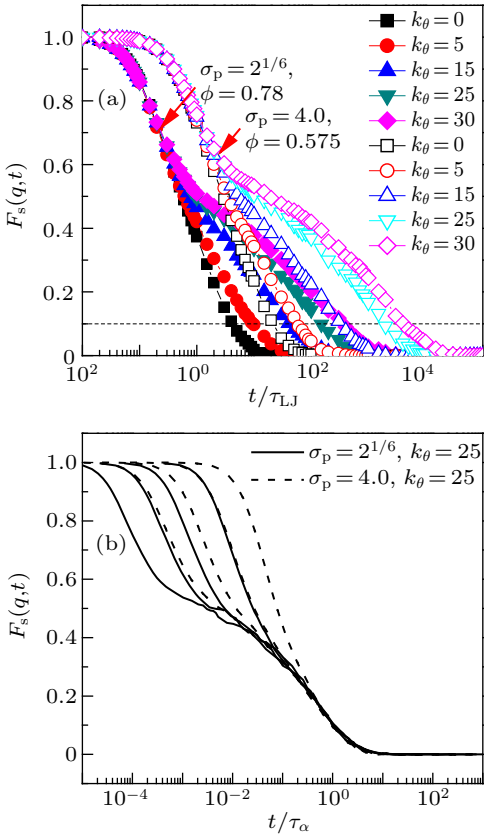


Fig. 6. The incoherent intermediate scattering function $F_s(q,t)$ for monomers. (a) The curves of $\sigma_p = 2^{1/6}$, $\phi = 0.78$ (solid symbols) and those of $\sigma_p = 4.0$, $\phi = 0.575$ (open symbols) for five chain stiffnesses. (b) The curves of $\sigma_p = 2^{1/6}$, $k_\theta = 25$ (solid line) for volume fractions (from left to right) $\phi = 0.80, 0.79, 0.78, 0.75$ and those of $\sigma_p = 4.0$, $k_\theta = 25$ (dashed line) for volume fractions (from left to right) $\phi = 0.575, 0.565, 0.55, 0.525$. q is chosen to be the value corresponding the first peak of the static structure factor. The relaxation time τ_α is defined as $F_s(q,t=t_\alpha) = 0.1$.

Figure 7 shows the variation of τ_α/τ_{LJ} as a function of bending constant k_θ for three monomer-size and volume-fraction combinations. τ_α/τ_{LJ} exponentially increases with k_θ, which can be well fitted by the formula

$$\tau_\alpha/\tau_{LJ} = \tau_\alpha^0/\tau_{LJ}\exp(\lambda k_\theta), \quad (6)$$

where τ_α^0/τ_{LJ} is the α relaxation time of bending constant $k_\theta = 0$, i.e., flexible chains. We obtain $\lambda = 0.15$ for $\sigma_p = 2^{1/6}$, $\phi = 0.78$ with $\tau_\alpha^0/\tau_{LJ} = 4.18$, $\lambda = 0.23$ for $\sigma_p = 2.0$, $\phi = 0.65$ with $\tau_\alpha^0/\tau_{LJ} = 13.27$, and $\lambda = 0.18$ for $\sigma_p = 4.0$, $\phi = 0.575$ with $\tau_\alpha^0/\tau_{LJ} = 21.65$. The Arrhenius behavior[47] is written as

$$\tau_\alpha(T) = \tau_0\exp\left(\frac{E}{k_B T}\right), \quad (7)$$

where E is the activation energy of the system. In our simulations, the reduced temperature is fixed at $T^* = 1.0$. Comparing the fitted formula and the Arrhenius behavior, we find that the increase of bending constant k_θ linearly increases the activation energy E of the colloidal-polymer system.

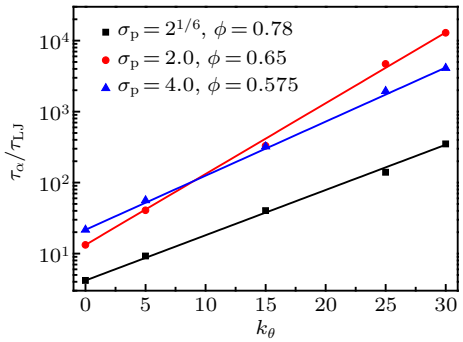


Fig. 7. Log-linear plot of τ_α/τ_{LJ} as a function of bending constant k_θ for three monomer-size and volume-fraction combinations, which is fitted by Eq. (6).

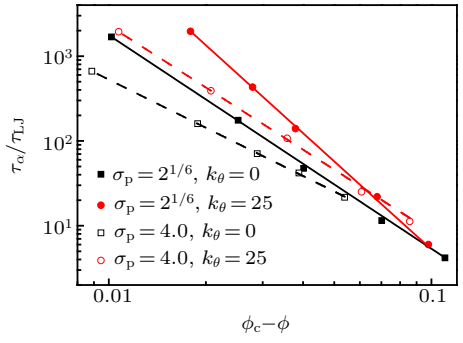


Fig. 8. The relations between the α relaxation time and volume fraction for four monomer-size and bending-constant combinations are fitted by Eq. (8).

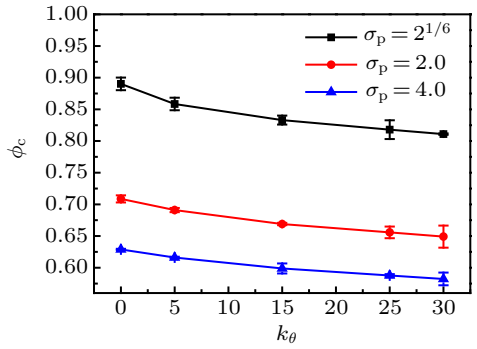


Fig. 9. The MCT critical volume fraction ϕ_c as a function of bending constant k_θ for three monomer sizes.

MCT theory predicts a power-law divergence of the α relaxation time as the MCT critical point is approached. For hard-sphere colloids, it is volume-fraction controlled and the power-law relation is written as

$$\tau_\alpha \propto (\phi_c - \phi)^{-\gamma}, \tag{8}$$

where $\gamma \approx 2.6$ and $\phi_c \approx 0.52$.[48] In Fig. 8, we fit τ_α by Eq. (8) for four monomer-size and bending-constant combinations. We obtain $\phi_c = 0.89$ and $\gamma = 2.52$ for $\sigma_p = 2^{1/6}$, $k_\theta = 0$; $\phi_c = 0.82$ and $\gamma = 3.44$ for $\sigma_p = 2^{1/6}$, $k_\theta = 25$; $\phi_c = 0.63$ and $\gamma = 1.89$ for $\sigma_p = 4.0$, $k_\theta = 0$; $\phi_c = 0.59$ and $\gamma = 2.44$ for $\sigma_p = 4.0$, $k_\theta = 25$. We also fit τ_α by Eq. (8) for the other monomer-size and bending-constant combinations, and the critical volume fraction ϕ_c decreases with bending constant k_θ for three monomer sizes (see Fig. 9).

3.4. Static and dynamic equivalences

In flexible colloidal-polymer systems, we find that the three colloidal-polymer systems ($\sigma_p = 2^{1/6}$, $\phi = 0.82$), ($\sigma_p = 2, \phi = 0.665$), and ($\sigma_p = 4, \phi = 0.59$) have the same hard-shpere equivalent volume fraction $\phi_{HS} = 0.503$ and the hard-shpere equivalent diameters are $\sigma_{HS} = 0.93$, 1.766, and 3.72, respectively.[30] At this equivalent volume fraction ($\phi_{HS} = 0.503$), the RDFs (static quantities) coincide well at distance beyond the first peak, and the date of dynamic quantities (MSDs) collapse well onto the master curves.

In Fig. 10, we check the static and dynamic equivalences of these three combinations in stiff-chain systems. For chains with bending constants $k_\theta = 5$ and $k_\theta = 15$, we find that the static RDFs do not coincide well because of the sharp maximums of the second peaks (see Figs. 10(a) and 10(b)), but the date of MSDs collapse well onto the master curves (see Figs. 10(c) and 10(d)).

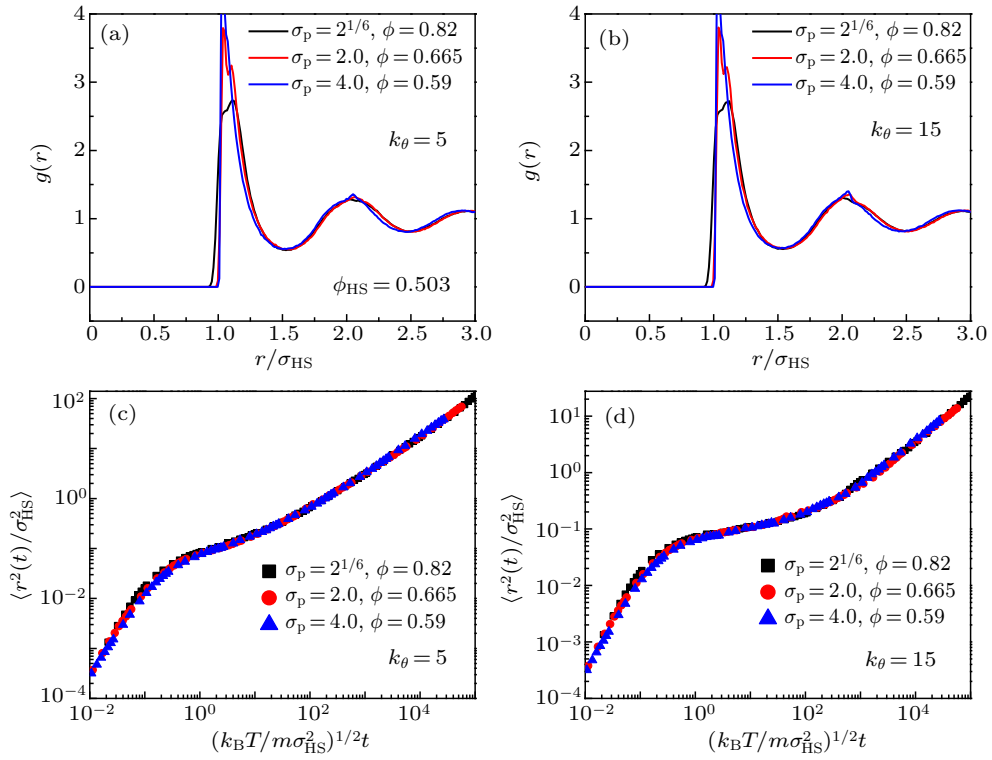


Fig. 10. Static and dynamic equivalences for combinations ($\sigma_p = 2^{1/6}, \phi = 0.82$), ($\sigma_p = 2$, $\phi = 0.665$), and ($\sigma_p = 4$, $\phi = 0.59$) in the stiff-chain systems. (a) and (b) The radial distribution functions for chains with bending constants $k_\theta = 5$ and $k_\theta = 15$. (c) and (d) The mean square displacements for chains with bending constants $k_\theta = 5$ and $k_\theta = 15$.

4. Summary

In this paper, we model colloidal polymer with chain stiffness. We focus on the quantitative differences in the static structure and glassy dynamics of the colloidal polymers between flexible chains and stiff chains. The two incompatible local lengths, i.e., monomer size and bond length, are manifested in the split of the first peak of RDF. For stiff chains, a sharp maximum appears in the second peak of RDF. In contrast to the very short-ranged intrachain correlation of flexible

chains, the average intrachain pair correlation function of stiff chains exhibits long-ranged periodic decayed peaks. The sub-diffusive exponent of the MSD of monomers increases with chain stiffness. For stiff chains with bending constant $k_\theta = 25$, when the volume fraction is above a threshold value ϕ^*, a caging regime emerges in the MSD. As anticipated, ϕ^* decreases with the increase of the monomer size: $\phi^* \approx 0.65$ for $\sigma_p = 2^{1/6}$, $\phi^* \approx 0.55$ for $\sigma_p = 2$, and $\phi^* \approx 0.49$ for $\sigma_p = 4$. If ϕ^* is used as the scaling unit for the volume fraction, the data of localization length versus volume fractions for different monomer sizes gather close to an exponential curve. The values of localization length of stiff chains are all larger and decay slower than those of flexible chains. Comparing the exponential fitted equation of the α relaxation time as a function of bending constant with the Arrhenius formula, it is found that the active energy of colloidal-polymer systems is linearly increased with the increase of chain stiffness. The α relaxation time of colloidal polymers can be well fit by the MCT power-law relation. The fitted values of ϕ_c are decreased with the increase of chain stiffness. Static and dynamic equivalences between stiff colloidal polymers of different monomer sizes have also been checked. We find that the curves of MSD can coincide well but the static RDF does not coincide well because of the sharp maximum of the second peaks. Finally, the model can be generalized to investigate more colloidal-polymer materials including the impacts of bond length, attractive force, and various topological structures.

References

[1] Michielettoa D and Turnerb M S 2016 *Proc. Natl. Acad. Sci. USA* **113** 5195
[2] Hsu H P and Kremer K 2019 *J. Chem. Phys.* **150** 091101
[3] Zirdehi E M andVarnik F 2019 *J. Chem. Phys.* **150** 024903
[4] Zhang B K, Li H S, Li J, Chen K, Tian W D and Ma Y Q 2016 *Soft Matter* **12** 8104
[5] Li J and Zhang B K 2019 *Chin. Phys. B* **28** 126101
[6] Baschnagel J and Varnik F 2005 *J. Phys.: Condens. Matter* **17** R851
[7] Barrat J L, Baschnagel J and Lyulin A 2010 *Soft Matter* **6** 3430
[8] Wang C, Chen Y C, Zhang S, Qi H K and Luo M B 2020 *Chin. Phys. B* **29** 108201
[9] Chen K and Schweizer K S 2007 *Phys. Rev. Lett.* **98** 167802
[10] Chen K and Schweizer K S 2009 *Phys. Rev. Lett.* **102** 038301
[11] Wan W B, Lv H H, Merlitz H and Wu C X 2016 *Chin. Phys. B* **25** 106101
[12] Paul W and Smith G D 2004 *Rep. Prog. Phys.* **67** 1117
[13] Bennemann C, Baschnagel J, Paul W and Binder K 1999 *Comput. Theor. Polym. Sci.* **9** 217
[14] Brodeck M, Alvarez F, Arbe A, Juranyi F, Unruh T, Holderer O, Colmenero J and Richter D 2009 *J. Chem. Phys.* **130** 094908
[15] Bernabei M, Moreno A J and Colmenero J 2008 *Phys. Rev. Lett.* **101** 255701
[16] Bernabei M, Moreno A J and Colmenero J 2009 *J. Chem. Phys.* **131** 204502
[17] Bulacu M and Giessen E V D 2007 *Phys. Rev. E* **76** 011807
[18] Bulacu M and Giessen E V D 2005 *J. Chem. Phys.* **123** 114901
[19] Bernabei M, Moreno A J, Zaccarelli E, Sciortino F and Colmenero J 2011 *J. Chem. Phys.* **134** 024523
[20] Bernabei M, Moreno A J and Colmenero J 2011 *J. Phys.: Condens. Matter* **23** 234119
[21] Hill L J, Pinna N, Char K and Pyun J 2015 *Prog. Polym. Sci.* **40** 85
[22] Gao B, Arya G and Tao A R 2012 *Nat. Nanotechnol.* **7** 433
[23] Yang M, Chen G, Zhao Y, Silber G, Wang Y, Xing S, Han Y and Chen H 2010 *Phys. Chem. Chem. Phys.* **12** 11850
[24] Zhao Y, Xu L, Marzan L M L, Kuang H, Ma W, Garcia A A, Abajo F J G D, Kotov N A, Wang L and Xu C 2013 *J. Phys. Chem. Lett.* **4** 641
[25] Bannwarth M B, Utech S, Ebert S, Weitz D A, Crespy D and Landfester K 2015 *ACS Nano* **9** 2720
[26] Guo D, Li C, Wang Y, Li Y N and Song Y L 2017 *Angew. Chem.* **129** 15550
[27] Vutukuri H R, Demirörs A F, Peng B, Oostrum P D J V, Imhof A and Blaaderen A V 2012 *Angew. Chem. Int. Ed.* **51** 11249
[28] Byrom J, Han P, Savory M and Biswal S L 2014 *Langmuir* **30** 9045
[29] Stuij S, Doorn J M V, Kodger T, Sprakel J, Coulais C and Schall P 2019 *Phys. Rev. Research* **1** 023033
[30] Li J, Zhang B K, Li H S, Chen K, Tian W D and Tong P Q 2016 *J. Chem. Phys.* **144** 204509
[31] Gleim T, Kob W and Binder K 1998 *Phys. Rev. Lett.* **81** 4404
[32] Tokuyama M, Yamazaki H and Terada Y 2003 *Phys. Rev. E* **67** 062403
[33] Berthier L, Biroli G, Bouchaud J P, Kob W, Miyazaki K and Reichman D R 2007 *J. Chem. Phys.* **126** 184503
[34] Hofling F, Munk T, Frey E and Franosch T 2008 *J. Chem. Phys.* **128** 164517
[35] Iacovella C R, Horsch M A and Glotzer S C 2008 *J. Chem. Phys.* **129** 044902
[36] Kremer K and Grest G S 1990 *J. Chem. Phys.* **92** 5057
[37] Paul W 2002 *Chem. Phys.* **284** 59
[38] Aichele M and Baschnagel J 2001 *Eur. Phys. J. E* **5** 245
[39] Bennemann C, Paul W, Binder K and Dünweg B 1998 *Phys. Rev. E* **57** 843
[40] Chen J X, Zhu J X, Ma Y Q and Cao J S 2014 *EPL* **106** 18003
[41] Li J, Zhang B K 2020 *EPL* **130** 56001
[42] There is no unique definition of the two ends of caging regime in the MSD curve. We mark the two ends by searching the points at which the slope of the log–log plot of the MSD curve reaches the average of the slopes of the caging regime and the sub-diffusive regime.
[43] Gotze W and Sjogren L 1992 *Rep. Prog. Phys.* **55** 241
[44] Fuchs M, Götze W and Mayr M R 1998 *Phys. Rev. E* **58** 3384
[45] Kim J, Kim C and Sung B J 2013 *Phys. Rev. Lett.* **110** 047801
[46] Schweizer K S and Saltzman E J 2003 *J. Chem. Phys.* **119** 1181
[47] Angell C A 1995 *Science* **267** 1924
[48] Gotze W 1999 *J. Phys.: Condens. Matter* **11** A1